Summer 8-15-2016

# Silk as a biomaterial paste for biomimetic composite

Sang Hyun Park
*Washington University in St Louis*

WASHINGTON UNIVERSITY IN ST. LOUIS
School of Engineering and Applied Science
Department of Materials Science and Engineering

Thesis Examination Committee:
Srikanth Singamaneni, chair
Parag Banerjee
Jeremiah Morrissey

# Silk as a biomaterial paste for biomimetic composite

by
Sang Hyun Park

A thesis presented to the School of Engineering
of Washington University in St. Louis in partial fulfillment of the
requirements for the degree of
Master of Science

August 2016

Saint Louis, Missouri

# Contents

List of Figures ..... iv

Acknowledgments ..... v

Dedication ..... vi

Abstract. ..... vii

Background ..... 1

Interfacial interaction effects on biomimetic composite of graphene oxide and silk ..... 3

2.1 Introduction ..... 3

2.2 Sample Preparation ..... 4

2.2.1 pH-dependent adsorption of silk on GO ..... 4

2.2.2 Graphene Oxide silk nanocomposite ..... 6

2.3 Buckling Compression Test ..... 6

Biomimetic layer-by-layer composite of chitin and silk ..... 9

3.1 Introduction ..... 9

3.2 Sample Preparation ..... 10

3.2.1 Chitin ..... 10

3.2.2 Chitin silk interaction ..... 11

3.2.3 Chitin silk nanocomposite ..... 12

3.3 Buckling Compression test ..... 14

Experimental Information ..... 18

A.1 Characterization ..... 18

A.2 Silk deposition on GO substrates for adsorption ..... 18

A.3 Graphene oxide Silk LBL assembly ..... 18

A.4 Chitin Silk LBL assembly ..... 19

A.5 Chitin Silk interaction study ..... 19

A.6 Mechanical Buckling Compression Test ..... 19

Synthesis Methods ..... 20

B.1 Materials ..... 20

B.2 Silk Fibroin Preparation ..... 20
B.3 Graphene Oxide Preparation ..... 20
B.4 Chitin Solution Preparation ..... 21
Supporting Information ..... 22
References ..... 28
Vita ..... 32

# List of Figures

**Figure 2.1- Schematics of Graphene oxide silk adsorption and AFM image of GO**.....4
**Figure 2.2- AFM images of different pH silk adsorption on GO flake**.....6
**Figure 2.3- Thickness variation depending on different pH of silk**.....7
**Figure 2.4- Buckling pattern and Moduli of different pH silk-GO composites**.....8
**Figure 3.1- Different concentration of chitin solution**.....10
**Figure 3.2- AFM images of low concentration chitin and different pH silk**.....12
**Figure 3.3- Schematic of chitin-silk bilayer**.....13
**Figure 3.4- Chitin-silk nanocomposite (10 bilayers)**.....14
**Figure 3.5- Buckling compression test of chitin silk film**.....16
**Figure S.1- Globule size of silk pH 4 and pH 7 on graphene oxide flake**.....22
**Figure S.2- Optical and AFM image of buckling pattern of GO silk composite**.....23
**Figure S.3- The amide peak deconvolution of chitin**.....24
**Figure S.4- AFM images of thicknesses of chitin silk composite**.....25
**Figure S.5- AFM images of morphology of chitin silk composite**.....26
**Figure S.6- Optical image of buckling pattern for chitin silk composite**.....27

# Acknowledgments

I would like to thank Professor Srikanth Singamaneni and Dr. Limei Tian for granting me the opportunity to experience and contribute to the Soft Nanomaterials Laboratory at Washington University in Saint. Louis. Also, special thanks to Ms. Sirimuvva Tadepalli and members of Soft Nanomaterials Lab for their help and support that encouraged me and pushed me to success.

Special thanks as well to Air Force Office of Scientific Research (S.S- Award # FA9550-15-1-0228) and (R.R.N- 12RX11COR) and AFRL/RX for their support.

Finally, I would also like to acknowledge those fellow graduate students and faculties from the MEMS department for their help as well as my friends who have supported me through this process.

*Sang Hyun Park*

Washington University in St. Louis
August 2016

Dedicated to my family for their unconditional support.

**ABSTRACT**

Silk as a biomaterial for biomimetic composite

by

Sang Hyun Park

Master of Science in Materials Science and Engineering

Washington University in St. Louis, 2016

Research Advisor: Professor Srikanth Singamaneni

Silk is a highly promising biomaterial with unique bio-physicochemical properties, such as excellent mechanical and optical properties, biocompatibility and programmable biodegradability. Among many different types, silk from domesticated silkworm, *bombyx mori* has received wide attention owing to its availability in virtually unlimited quantities and ease of extraction. In this study, we investigated silkworm silk as a protein glue to realize nacre-like composites. We have employed spin assisted layer-by-layer technique to fabricate ultrathin free-standing biocomposite films. Two different composites have been studied: (i) graphene oxide (GO)/silk and (ii) chitin/silk. From our prior work, it is known that the adsorption of amphiphilic silk on amphiphilic GO flakes is highly sensitive to the pH of the silk solution. In this study, we investigated the influence of pH of the silk solution on the mechanical properties of silk/GO composites. We found that the pH of silk solution has a significant influence on the structure and elastic modulus of the composite films. Over the pH rage studied here (pH4 to pH10), the modulus of composite films could be varied from 8 GPa to 31 GPa. Apart from the relative volume fractions of the two components, our results show that interfacial interaction between protein glue and graphene oxide plays a determining role in the ultimate mechanical properties of the film.

Additionally, we fabricated first protein-polysaccharide biocomposite layer-by-layer assembled composite using silk and chitin. Chitin is known for its chemical stability and excellent

mechanical properties. However, it is a very difficult material to process due to its poor solubility, requiring strong organic solvent of hexafluoro-2-proponal (HFIP) to dissolve. Despite these difficulties, we have successfully developed a robust fabrication approach to realize chitin-silk biocomposite with different volume fractions of chitin, and demonstrate the release of these film from substrate into freestanding state. We have investigated the mechanical properties of these ultrathin films. The highest elastic modulus of the composite was found to be 6.9 GPa with 0.3% chitin, which is significantly higher than that of the composite film made with chitosan, a highly deacetylate form of chitin.

Taken together, our studies provide novel insights into the nanoscale structure and mechanical properties of ultrathin free-standing bionanocomposites fabricated using layer-by-layer assembly.

# Chapter 1

# Background

Silk fibers are among the strongest natural polymeric materials with a unique combination of high modulus and high elongation at failure. [1] In the silk from silkworm, *Bombyx mori*, crystalline β-sheet regions are formed due to the presence of GAGAGS repeats, with poorly ordered domains segregating to form hierarchical order-disorder structures. This staggered architecture plays a key role in increasing the toughness of silk fibers to record values. The mechanical properties of silk materials strongly depend on their secondary structure. A freshly prepared aqueous solution of reconstituted silk fibroin typically presents an amorphous random coil secondary structure, often termed as silk I, characterized by crank-shaft conformation. Both amorphous silk and silk I are water soluble, however, when subjected to organic solvents such as methanol, water vapor, heat and or mechanical strain, they can crystalize and convert to extremely stable and water insoluble silk II. [2] Silk II is characterized by a beta pleated sheet structure stabilized by inter-chain hydrogen bonding, showing an increased elastic modulus and mechanical strength compared to silk I. The tendency of aqueous silk fibroin solution to form opaque gels over long periods of time is attributed to the formation of stable β-sheets which serve as physical crosslinks between the silk chains. [3] The physical crosslinks in silk hydrogels resulting in stable β-sheets can be induced by shearing (spinning), water evaporation (or water exclusion from the bulk via osmotic stress), solvent exposure, or heating which take an unusually long time. [3]

Another reason it is an excellent biomaterial is that *Bombyx mori* silkworm silk can be easily processed into multiple different forms such as solution, electro spun fibers, hydrogels, freeze dried aero-foams can be obtained. [4]

Ease of processing is extremely important in realizing nanocomposites for real-world applications. For instance, a biomaterial with excellent properties such as chitin, which will be discussed later, is very difficult to process due to its chemical inertness. Although the excellent properties have been widely recognized, it has not been widely employed in the fabrication of biocomposites due to the difficulties associated with dissolving and processing chitin. On the other hand, silkworm silk can be easily processed into multiple forms. Silk has been widely employed as a

protein polymer in numerous applications including nacre mimetic composites. Nacre is an excellent example of nanoscale engineering in nature that results in supreme mechanical properties such as high strength and excellent toughness. Most conventional way to achieve nacre-like structure is to create composite using layer-by-layer (SA-LbL) assembly approach. Especially, spin assisted layer-by-layer approach allows to control over the film thickness, internal organization, and molecular structures. As a result, by using SA-LbL technique with silk solution, a uniform nanocomposite of silk nacre like biomimetic composite can be fabricated. [5-6] In this work, for the first time, we demonstrate a layer-by-layer assembly of silk and chitin with a precise control of thickness and internal structures. Importantly, we demonstrate ability to freely suspend ultrathin LbL assembled films of chitin/silk composite and probe their mechanical properties.

# Chapter 2

# Interfacial Interaction Effects on Biomimetic Composite of Graphene Oxide and Silk

## 2.1 Introduction

To advance the emerging field of biotic/abiotic hybrids and bioenabled materials, it is extremely important to understand the interfacial interactions between biological materials and synthetic nanomaterials. The interface between dissimilar materials, e.g., hard/soft and biotic/abiotic, critically determines the properties and the ultimate performance of the bionanocomposites.[7] For example, within a layered composite, the interfacial interactions between a small amount of soft polymeric material and hard inorganic material has been identified to be largely responsible for the remarkable toughness of natural biocomposite structures, such as nacre, and is a critical design consideration in the fabrication of artificial nacre mimics.[8-10] The toughness of the nacre mimetic composites is due to the energy dissipation that occurs during the stretching and unfolding of the polymeric chains between and within the bricks, causing grain reorientation and crack deflection before failure.[11]

Recently, many researchers have focused on graphene oxide (GO) for nacre mimics due to its unique properties. GO has impressive mechanical property. It has a tensile modulus of ~0.25 TPa; [6] a large surface to volume ratio, which maximizes interfacial interactions; [12] high water solubility as well as a tendency to form a 2D layered sheet like structure. [13,14] Silk has been known as an excellent biopolymeric glue for the fabrication of nacre mimics and biocomposites, because of its multi-domain structure, with repetitive motifs that facilitate the formation of highly stable anti-parallel β-sheets, amphiphilic nature and virtually unlimited supply. [15,16] Our group thoroughly studied how adsorption behavior of silk differs on GO flakes depending on its pH. Through adsorption study, we found that there were higher levels of silk adsorption on GO flakes when silk pH was low, compared to when it was high. [18]

We fabricated a graphene oxide silk biomimetic composite using spin assisted layer-by-layer (SA-LBL) assembly method. By using a polystyrene sacrificial layer, we demonstrated the ability to

fabricate a free-standing film that can be transferred onto a different surface. We hypothesized that by controlling the pH of silk that was layered with graphene oxide, we could change the adsorption behavior of silk solution on the GO flake, which would ultimately change the interfacial interaction within the layers of the composite, and the mechanical properties of the composites.

## 2.2 Sample Preparation

### 2.2.1 pH-dependent Adsorption of Silk on GO

To probe the adsorption of the silk fibroin on the surface of GO, we deposited GO on a silicon substrate. Commercially available GO flakes were filtered using a 5 μm filter to remove large aggregates and spin coated on a silicon substrate. (Fig.2.1 B) When single monolayers of GO were achieved on silicon substrates, we exposed the substrates to different pH silk solutions to observe the adsorption behaviors. (Fig.2.1 A)

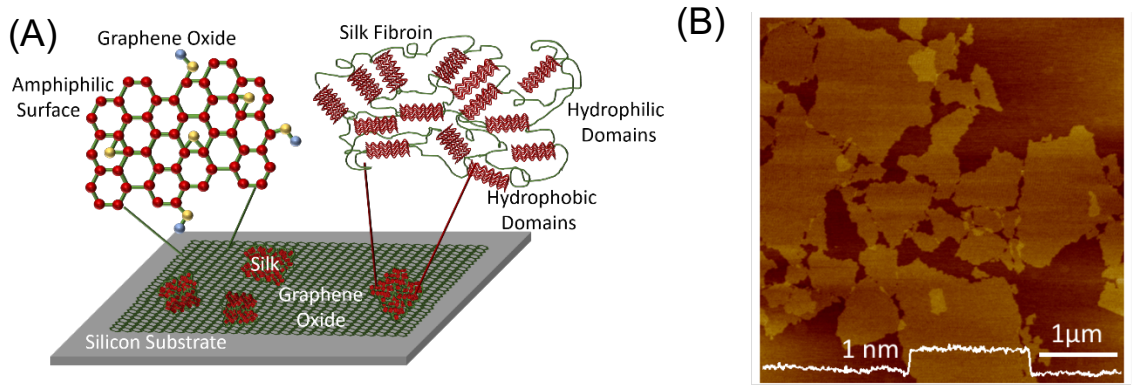


**Figure 1: (A) Schematic showing the interaction between graphene oxide and silk. (B) AFM image showing the GO flake size. Height Scale is 10nms**

At pH 4, we observed a very high density of silk chains adsorbed on the surface of GO due to polar and hydrophobic interactions (Fig.2.2 A, E). The close to zero zeta potential of the silk at pH 4 also resulted in intermolecular attraction between the silk chains through hydrophobic and van der Waals interactions. Hence, most of the globules of silk are possibly comprised of more than one chain of the silk fibroin. As the pH is increases, the amount of silk on the GO reduces and the distance between the silk globules also increases. At pH 7, due to the negatively charged state of the

silk (zeta potential of -14 ± 2 mV), electrostatic repulsion between the silk and GO dominates the adsorption process (Fig.2.2 D, H). The electrostatic repulsion between the silk chains and oxidized domains of GO forces the adsorption of silk on the deoxidized hydrophobic domains of GO through hydrophobic interactions. In addition, intermolecular electrostatic repulsions prevent the silk chains from approaching each other thus increasing the distance between the silk globules adsorbed on the GO surface. The average distance between the silk globules adsorbed on GO increases upon increasing the pH of the silk, which can be attributed to the distributed hydrophobic domains of GO and the intermolecular electrostatic repulsions of the negatively charged silk at pH 7 (Fig.2.2 (A-H)).

We noted that the adsorption of the silk on a silicon surface also appears to be highly pH-dependent. A silicon surface with the native oxide layer is rich in hydroxyls groups and exhibits a negative charge. The density of the silk adsorbed on the silicon surface was found to progressively decrease with increasing pH (Fig.2.2 (A-D)). At pH 4 and pH 5, the presence of silk on a silicon surface is evident, but the concentration of silk reduces significantly at pH 6. At pH 7, the negative charge of the silk resulted in virtually no adsorption on the silicon surface.

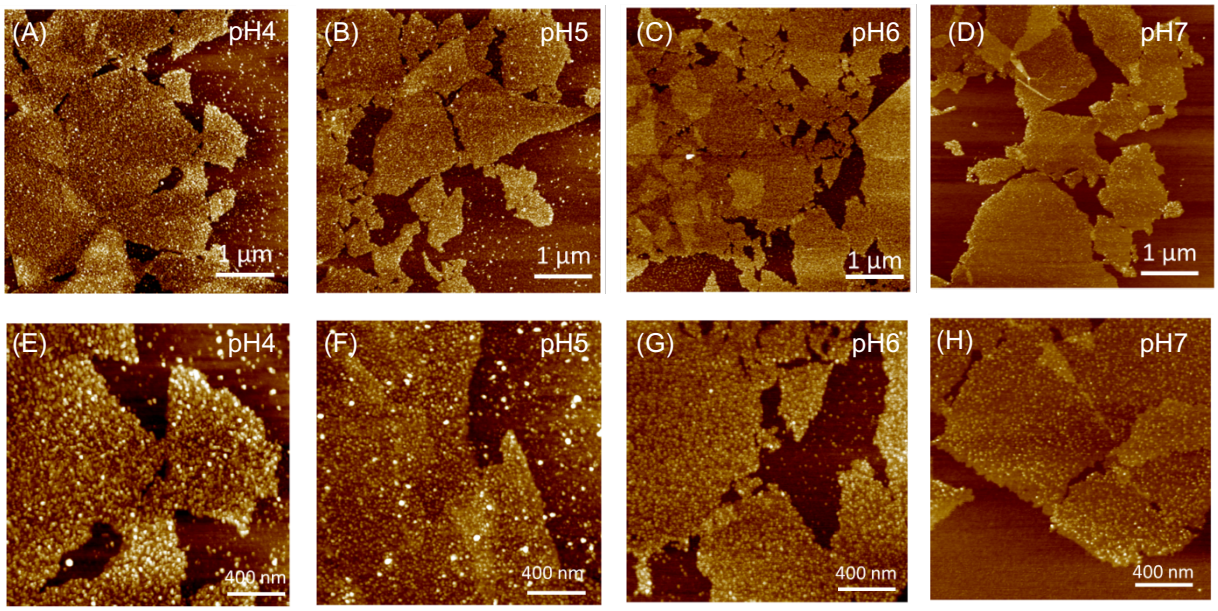


**Figure 2.2: The adsorption of silk on GO on silicon substrate at different pH values; (A, E) pH 4 (B, F) pH 5 (C, G) pH 6 (D, H) pH 7. Height Scale is 10 nm.**

### 2.2.2 Graphene Oxide Silk Nanocomposite

Unlike the adsorption study, in this study graphene oxide was synthesized using graphite powders to fabricate the composite. GO flakes were obtained using a method recently reported by Tour and co-workers. [35] The reason to synthesize the GO flakes was to have more precise control of the flake size.

Different pH of 0.2% silk were achieved through careful modification using the pH probe. In this study pH 10 silk, pH 7 silk and pH 4 silk were observed considering pH 10 silk and pH 4 silk as two opposite extremes. For each pH, layer-by-layer film was fabricated by using alternate layers of GO and silk. To understand the thickness increment over the number of layers, scratch tests were performed for every two layers. Every bilayer, the increment in thickness for pH10 composite was significantly lower than the other two pH conditions. The AFM images of GO silk film with 10 bilayers shows the morphology of the graphene oxide and the adsorbed silk on the surface. (Fig.2.3 A, B).

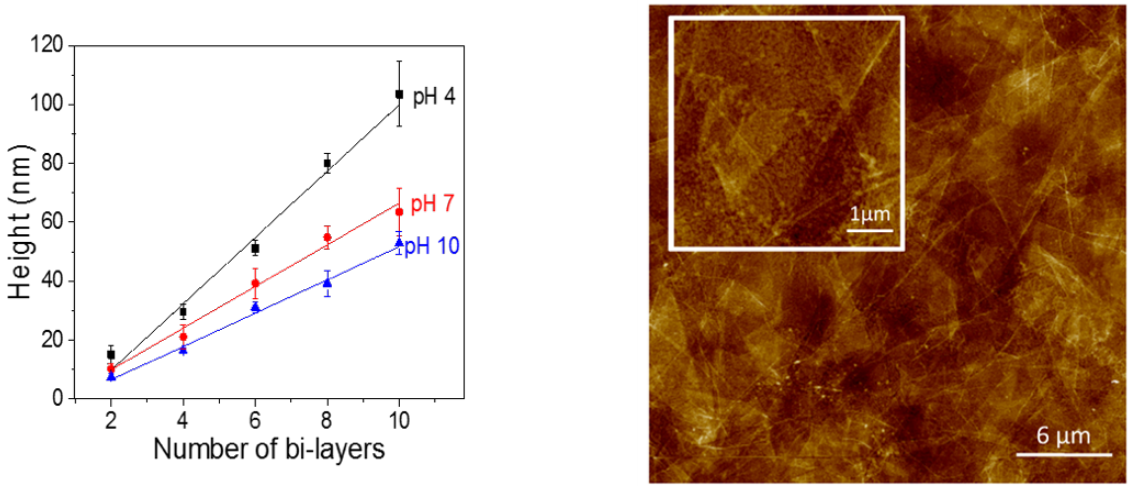


**Figure 2.3: (A) Number of bilayers vs thickness of varying pH of silk (B) AFM image of GO silk nanocomposite film pH10**

## 2.3 Buckling Compression Test

The nanocomposite films were fabricated on a polystyrene (PS) sacrificial layer. The sacrificial layer can be removed using toluene to release the composite film. The composite film is

fabricated with alternative silk and GO layers with differing pH values of silk. In order to probe the elastic modulus, the free-standing film was transferred onto a compliant polydimethylsiloxane (PDMS) substrate. The elastic modulus of the go-silk film was determined using strain-induced elastic buckling instability for mechanical measurement. [17] Briefly, subjecting a compliant polymer substrate to a compressive stress, results in a spontaneous periodic buckling pattern. [18] The buckling wavelength is given by equation [19]:

$$\lambda = 2\pi t \left[\frac{(1-v_s^2)E_f}{3(1-v_f^2)E_s}\right]^2$$

Where $\lambda$ is the wavelength of the periodic buckling pattern, $E_f$ and $v_f$ are the elastic modulus and the Poisson's ratio of the film, and $E_s$ and $v_s$ are the elastic modulus and the Poisson's ratio of the PDMS substrate and $t$ is the thickness of the film.

The freely standing go-silk film was transferred onto a compliant PDMS surface which was subjected to a compression resulting in the uniform buckling of the film. The optical images revealed large regions of periodic wrinkles with a uniform spacing (Fig. 2.4. A). Fast Fourier transform (FFT) of the optical images was employed to determine the wavelength of the buckles to be 7.4±0.1 μm. Using equation (1), the Young's modulus of the pH10 GO-silk layered films was calculated to be 31.1±1 GPa. The Young's modulus as a function of pH of the silk was plotted (Fig.2.4. B). An increase in pH of the silk in the layered go-silk composite resulted in an increase in the modulus. This phenomenon can be attributed to the increase in the binding interactions among graphene oxide and with the silk film.

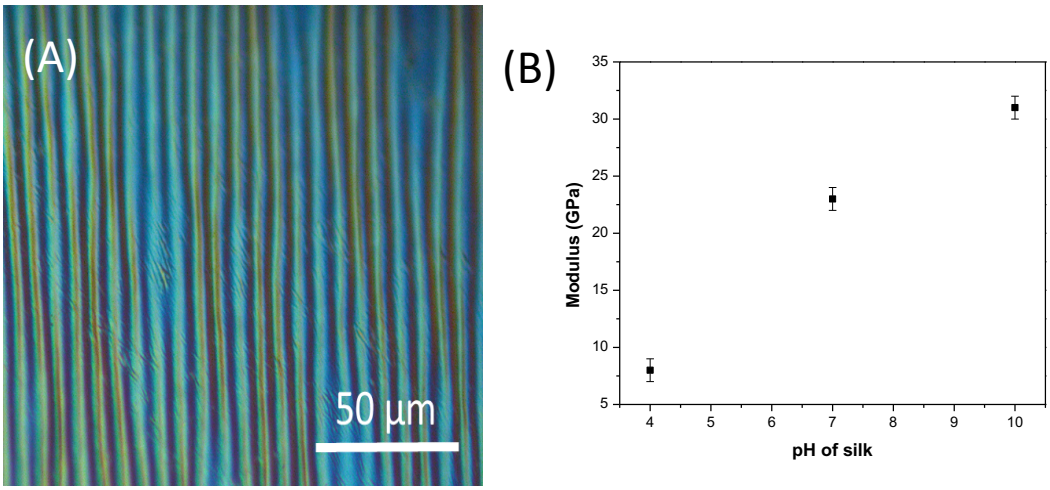


**Figure 2.4: (A) Optical micrograph of a buckled free stand film (B) Moduli of different pH GO-silk films**

# Chapter 3

# Biomimetic Layer-by-Layer Composite of Chitin and Silk

## 3.1 Introduction

Nature exhibits distinctive mechanical properties due to the unique physical and chemical interactions among its biomolecular components at the nanoscale. [20] The intricate structural components of an insect cuticle, mollusk nacre and crustacean exoskeleton, for example, rely on the interactions between chitin polysaccharides and proteins to demonstrate an unusually high strength and toughness. [21] The proteins that exist in insect cuticles are a diverse class of cuticle like structural proteins including fibroin, elastin, abductin and collagen, which have a high content of glycine and alanine. [22]

Chitin is the world's second most resourceful polysaccharide after cellulose that has structural repeat units of β-(1,4) N-Acetyl-D-glucosamine. Chitin is mechanically stable, biodegradable, non-toxic and physiologically inert and is used in a variety of biomedical applications including tissue engineering, scaffolds, neural networks, wound dressing and biocompatible devices. [24-26] Its crystal structure is in ordered crystalline nanofibers with hydrophobic interactions between glucosamine rings and hydrogen bonding along the linear chains. This strong bonding between the chains results in the insoluble nature of chitin in water and common organic solvents. [23]

The organic part of insect cuticle is made up of chitin nanofibers embedded in silk-like protein matrix. [27] Artificial biomimetic composites based on chitin and silk are difficult to engineer due to the lack of structural basis for their interactions and the low solubility of chitin in most organic solvents. [28] However, chitin can be dissolved using Hexafluoroisopropanol (HFIP), which is very strong toxic organic solvent.

In this study, we fabricated a chitin silk biomimetic composite once again using the spin assisted layer-by-layer (SA-LBL) assembly method. By using a polystyrene sacrificial layer, we demonstrated that the fabricated composite film can be freely suspended. By controlling the

concentration of chitin and silk and the number of layers, we were able to control the thickness and the mechanical properties of the mechanical composites. This will be the first demonstration of a structural composite of chitin and silk composite with a distinct laminar boundary resembling the laminar structure of a natural cuticle.

# 3.2 Sample Preparation

## 3.2.1 Chitin

The first studies on chitin film were done on silicon substrates. When chitin films are fabricated by spin assisted deposition of chitin in HFIP on a silicon surface, the thickness of the chitin film increases as the concentration of the chitin solution increased. The deposition of chitin film at a low concentration (0.1 - 0.2 %) resulted in the formation of a porous film with chitin nano-fibers (Fig. 3.1 A-B). As the concentration of chitin solution increases, the film becomes less porous (Fig. 3.1 C-E) and the thickness of the chitin film increases correspondingly (Fig. 3.1 F).

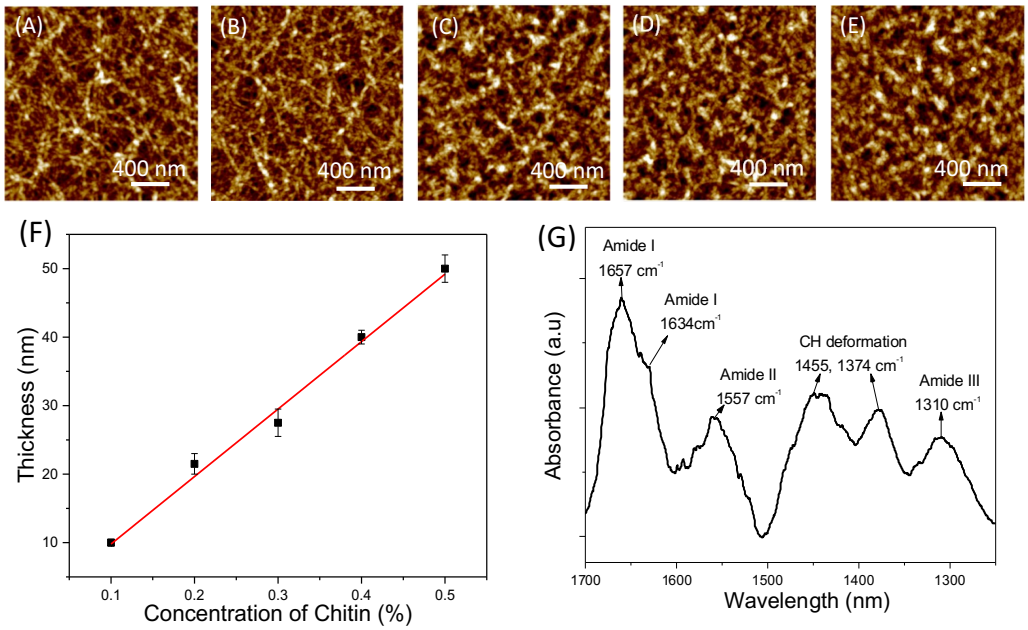


**Figure 3.1: AFM images of the chitin film spin coated from (A) 0.1% (B) 0.2% (C) 0.3% (D) 0.4% (E) 0.5%. Z-scale: 20 nm (F) Thickness of the nanoscale films increasing with the concentration of chitin used for spin coating. (G) IR absorption spectra of the nanoscale chitin film.**

The thickness of the chitin film increased from 10 nm to 50 nm by increasing the concentration of chitin from 0.1% to 0.5% as measured by the AFM scratch test (Fig. S.1). A further increase in concentration of chitin beyond 0.5% resulted in a solution with a very high viscosity, further resulting in the non-uniformity of the fabricated film. Fourier transform infrared spectroscopy (FTIR) provides insight into the structure of the chitin film. The characteristic peaks of chitin are observed at 1657 $cm^{-1}$(amide I), 1557 $cm^{-1}$(amide II) and 1310 $cm^{-1}$(amide III). [29] The presence of α-chitin is confirmed by the presence of amide-I (C=O stretching) split peaks at 1657 $cm^{-1}$ and 1634 $cm^{-1}$. The peak at 1657 $cm^{-1}$ corresponds to the hydrogen bonding of the C=O group of chitin with the –NH group of the adjacent chitin, while the peak at 1634 $cm^{-1}$ corresponds to the hydrogen bonding of C=O group of chitin with the –OH group of the adjacent chitin. The higher intensity of the 1657 $cm^{-1}$ when compared to 1634 $cm^{-1}$ suggests that the intermolecular hydrogen bonding is significantly established through the C=O and the –NH groups. Additionally, the peak at 1635 $cm^{-1}$ corresponds to the C=O groups of the six chitin molecules on the surface of the chitin nanofibers that do not participate in the intermolecular hydrogen bonding.

### 3.2.2 Chitin Silk Interaction

In order to understand the interaction of chitin and silk, we used chitin fibers spin casted from a low concentration of chitin solution in HFIP (Fig. 3.2 A, D). The sparsely distributed chitin nanofibers of α-chitin have a diameter of 2.7±0.7 nm with a varying degree of the self-assembly process which is similar to the reported values. [30] The biogenic nanofibers found in the tissues of living organisms such as shrimp shells and anthropod cuticles have a similar length and diameter. [31] The adsorption of silk on chitin fibers is dependent on the pH of the silk solution used for adsorption. [32] As the isoelectric point of silk is close to pH 4, the silk fibroin chains adsorb on the chitin fibers at a high density (Fig. 3.2 B, E). However, at pH 10, the adsorption of silk on chitin fibers is not high due to the intermolecular electrostatic repulsions caused by negatively charged silk fibroin (Fig. 3.2 C, F). These interactions can be modulated by tuning the pH of silk which can be used in the design of layer-by-layer biomimetic composites of chitin and silk.

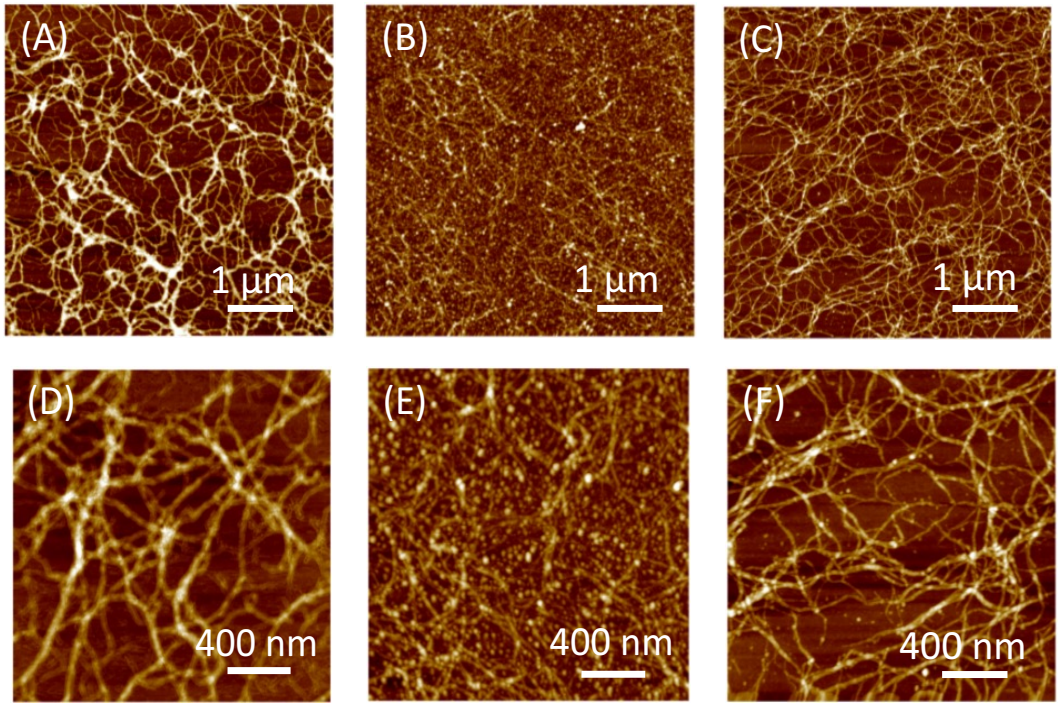


**Figure 3.2: AFM images of chitin fibers (A, D) without silk adsorption (B, E) silk adsorption from pH 4 (C, F) silk adsorption from pH 10. Z-scale: 20 nm.**

### 3.2.3 Chitin Silk Nanocomposite

The chitin silk layer-by-layer film was fabricated by using alternate layers of chitin in HFIP and silk film followed with methanol treatment. Methanol treated silk is resistant to aqueous and organic solvents preventing the desorption of the silk upon exposure to HFIP. [33] HFIP is a strong organic solvent capable of desorption of methanol treated silk upon exposure for long periods of time. Therefore, we used a silk film with a minimum thickness of 15 nm such that the HFIP exposure during the spin coating does not dissolve the silk layer. We deposited alternate layers of chitin and silk were deposited to fabricate a layer-by-layer assembly of silk and chitin of 10 bilayers (Fig. 3.3).

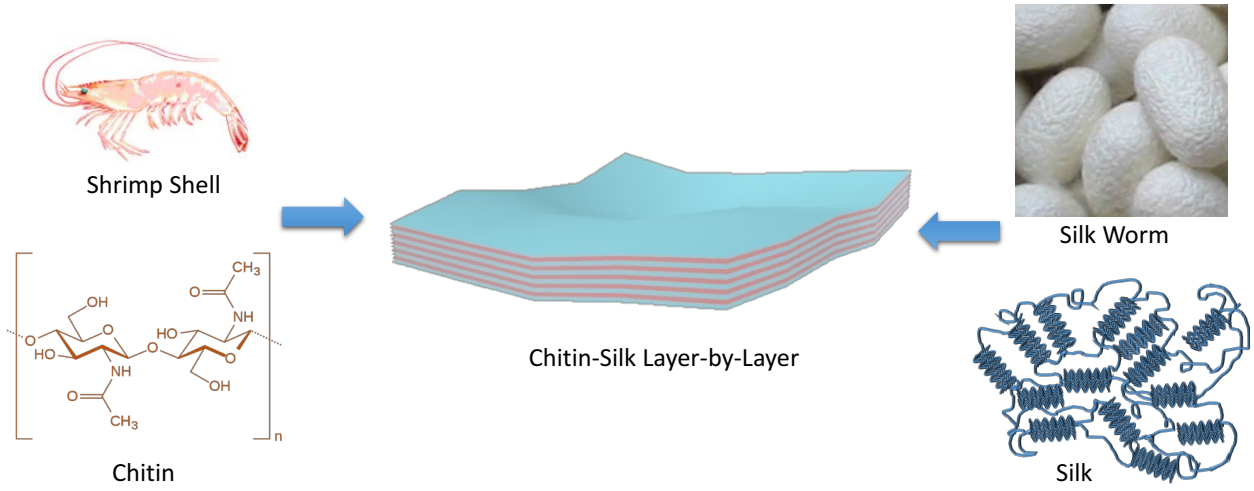


**Figure 3.3: Schematic showing fabrication of chitin and silk biomimetic composite. Silk extracted from silk worm cocoons and chitin extracted from squid are used to fabricate the chitin-silk layer-by-layer biomimetic composite.**

The thickness of the film increased linearly with the number of bilayers, the main characteristic of layer by layer deposition (Fig. 3.4 C). The AFM images of chitin silk film with 10 bilayers shows the morphology of the chitin fibers and the adsorbed silk (Fig. 3.4A, B). The FTIR spectrum (Fig. 3.4 D) collected from chitin shows the peak at 1657 $cm^{-1}$ is attributed to the hydrogen bonding interaction of the C=O group to the –NH group of the adjacent chitin chain. The silk film also showed amide I band at 1657 $cm^{-1}$ corresponding to the intermolecular hydrogen bonding. The chitin silk layer-by-layer showed an increase in intensity of the amide I peak which is higher than the simple sum of chitin and silk spectra. The increase in amide I peak might indicate the possible additional hydrogen bonding between the C=O group of chitin and the –NH group of the silk. Further, the peak from amide III of chitin at 1310 $cm^{-1}$ shifted to higher frequencies in the chitin silk 10 bilayer film.

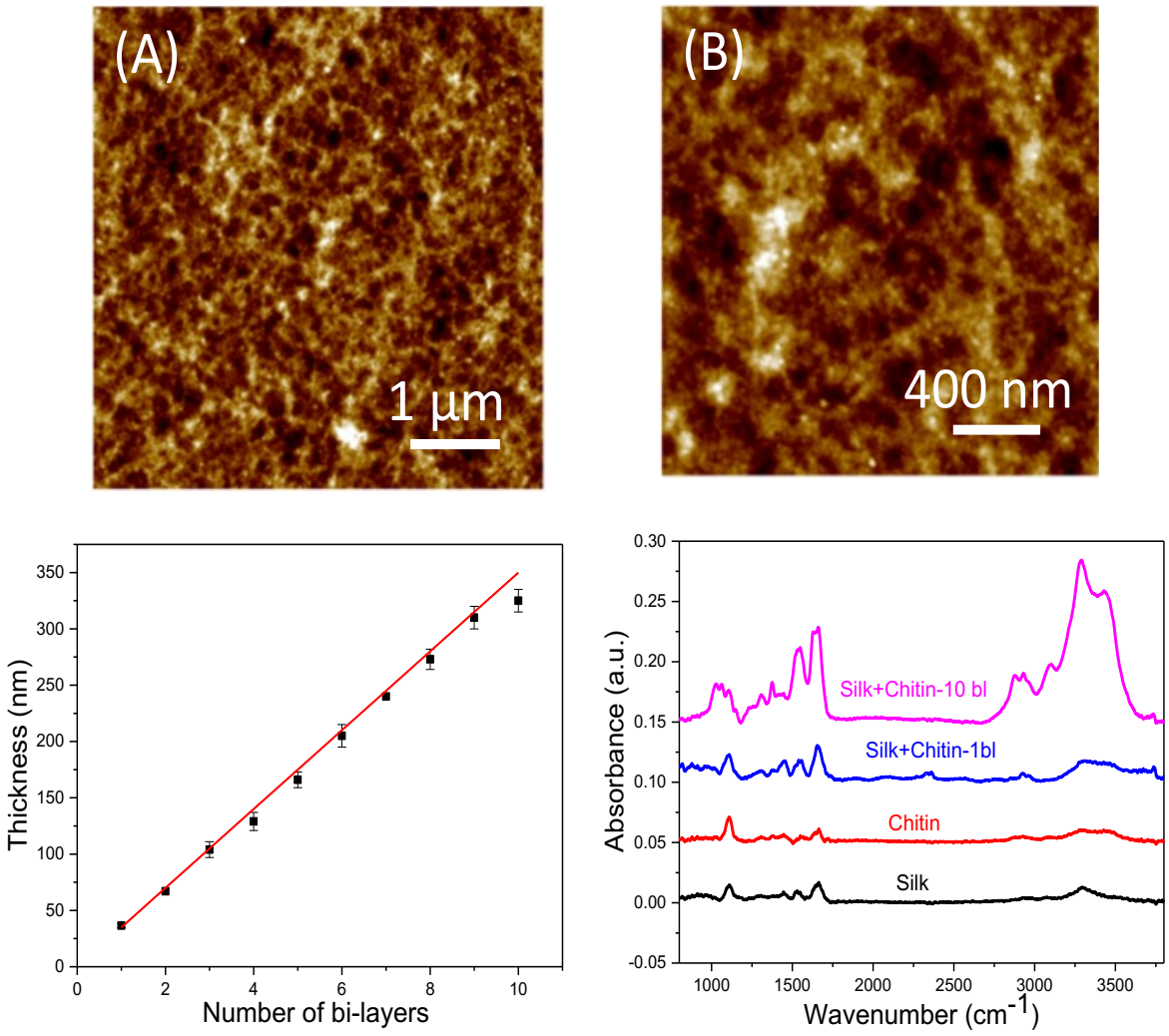


**Figure 3.4: (A, B) AFM images of 10 bilayers of chitin and silk. Z-scale: 20 nm. (C) Thickness of the chitin-silk films as a function of number of bi-layers. (D) IR absorption spectra of chitin and silk bilayers.**

## 3.3 Buckling Compression Test

The nanocomposite films were fabricated on a polystyrene (PS) sacrificial layer. The sacrificial layer can be removed using toluene to release the composite film. It is shown that the film is free-standable by releasing the film on to the TEM grid with ~200 µm apertures (Fig. 3.5B). For the modulus study, we fabricated silk-(chitin-silk)2-silk composite. The top and bottom silk films were layered to have symmetric structure. The freestanding film was also released onto polydimethylsiloxane (PDMS) substrate. The elastic modulus of the film was determined using

strain-induced elastic buckling instability for mechanical measurement. [17] Briefly, subjecting a compliant polymer substrate to a compressive stress, results in a spontaneous periodic buckling pattern. [18] The buckling wavelength is given by: [19]

$$\lambda = 2\pi t \left[\frac{(1-\upsilon_s^2)E_f}{3(1-\upsilon_f^2)E_s}\right]^2$$

Where $\lambda$ is the wavelength of the buckling pattern, $E_s$ and $\upsilon_s$ are the elastic modulus and the Poisson's ratio of the PDMS substrate and $E_f$ and $\upsilon_f$ are the elastic modulus and the Poisson's ratio of the chitin-silk film and t is the thickness of the film.

The free standing chitin silk film was transferred onto PDMS surface, which was compressed to create uniform buckling of the film. The optical images of the PDMS surface show large regions of periodic wrinkles with a uniform spacing (Fig. 3.5. C). Fast Fourier Transform (FFT) of the optical images was employed to determine the wavelength of the buckles to be 11±0.1 μm. The Young's modulus of the chitin silk layered films was calculated to be 6.9±0.1 GPa. The Young's modulus as a function of chitin concentration was plotted (Fig.3.5. D). An increase in volumetric concentration of the chitin in the layered chitin-silk composite resulted in an increase in the modulus. This phenomenon can be attributed to the increase in the binding interactions among chitin nanofibers film and with the silk film.

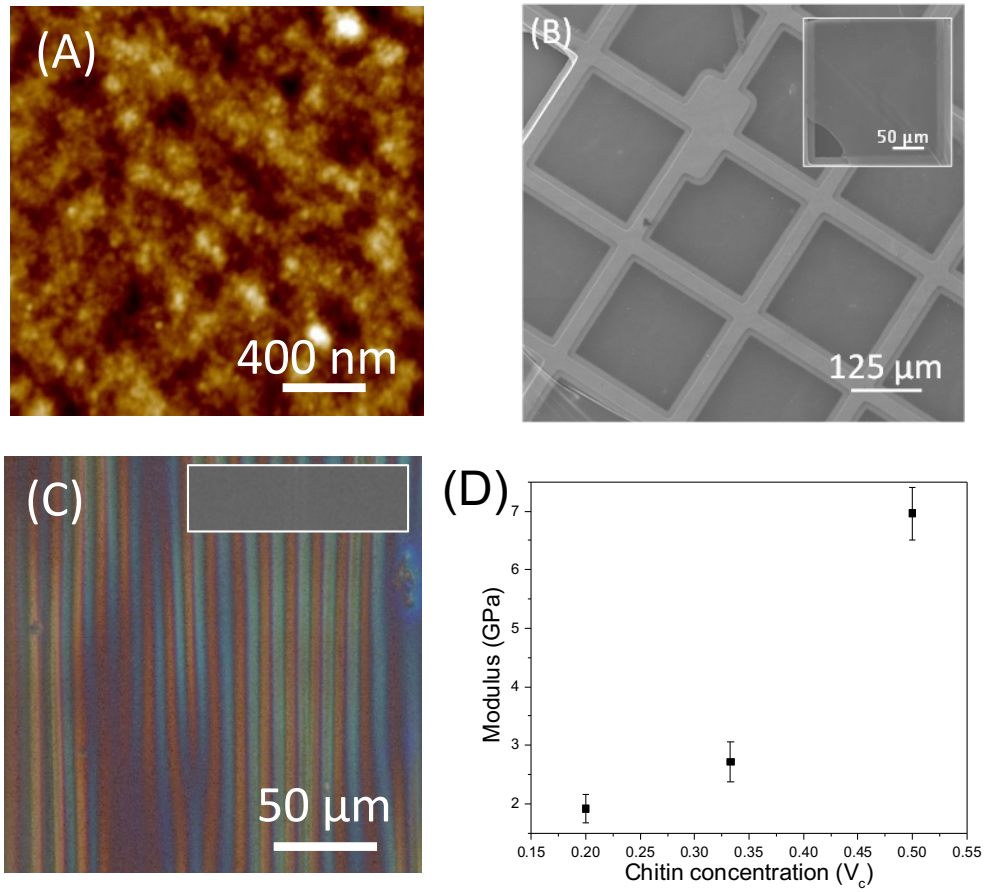


**Figure 3.5: (A) AFM images of chitin-silk layer-by-layer free standing film (Z-scale: 20nm) (B) SEM image of the film transferred onto a grid. Inset showing an intentionally ruptured film. (C) Optical micrograph of a buckled free standing film. (D) Elastic modulus of the free standing film as a function of chitin concentration.**

On the basis of fiber composite theory, the Young's modulus of the biocomposite film based on the rule of mixtures is $E = E_f V_f + E_m V_m$ where $E_f$ and $E_m$ are the Young's modulus of the fiber and matrix respectively and $V_f$ and $V_m$ are the volume fractions of the fiber and the matrix respectively. The Young's modulus of the biocomposite film with 0.3 wt% chitin (6.9±0.1 GPa) which is higher than that predicted by the rule of mixtures (E = 2 GPa). The high Young's modulus when compared to the values predicted in literature is attributed to the ability to engineer to separate

phases organized in an ordered laminate structure and the intermolecular hydrogen bonding between chitin and silk as confirmed by the FTIR measurements. This will be the first demonstration of a structural composite of chitin and silk composite with a distinct lamellar boundary resembling the structure of natural cuticle.

# Appendix A

## Experimental Information

## A.1 Characterization

Atomic Force Microscopy (AFM) images were captured using Dimension 3000 (Bruker) in light tapping mode. A V-shaped silicon cantilever with AFM tips (Micromash) with a nominal tip radius of 8nm were used for the imaging the samples. FT-IR spectroscopy measurements were performed using a Nicolette Nexus 470 using a Praying Mantis Harrick that is used to get a diffuse reflectance IR Fourier transform 1024 scans at a resolution of $1cm^{-1}$. Scanning Electron Microscopy (SEM) images were captured using a FEI Nova 2300 Field Emission SEM with an accelerating voltage of 10kV.

## A.2 Silk Deposition on GO Substrates for Adsorption

Commercially available graphene oxide was dispersed in water (0.1 mg/mL) and sonicated for one hour to prevent the formation of clusters. The resulting suspension was filtered using 5.0 μm polycarbonate filters. The resulting solution then was spin coated on silicon wafers that are cleaned in piranha solution. The GO substrate was immersed in a 0.01 wt% silk solution of the desired pH. In a typical preparation, the substrate was rinsed with Nano-pure water after 30 seconds (unless otherwise stated) and dried for further characterization.

## A.3 Graphene oxide Silk Layer-by-Layer Assembly

Initially, the polystyrene sacrificial layer (about 100nm) was deposited on a clean silicon wafer. Before spin coating any silk solutions, the pH values of silk solutions were tuned to set pH (pH4, pH7, pH10). Then the silk solution (0.2%) of set pH is spin coated (3000rpm, 30sec) and graphene oxide was spin coated next. Then Nano-pure water was spin coated to rinse away any excess material left on the surface. This steps were repeated until wanted number of bilayers were achieved.

## A.4 Chitin Silk Layer-by-Layer Assembly

Initially, the polystyrene sacrificial layer (about 100nm) was deposited on a clean silicon wafer and the silk solution (0.5%) was then spin coated (3000rpm, 1 m). Methanol treatments were done after every silk solution deposition by submerging the substrate in methanol for 3 minutes and letting it dry naturally at room temperature. Then silk solution (0.5%) and chitin solution (0.15%) were deposited alternatively on the substrate. After two of each layer's deposition, silk solution (0.5%) was deposited again and treated with methanol, resulting in a silk-(silk-chitin)$_2$-silk film.

## A.5 Chitin silk interaction study

0.01% chitin solution is spin coated on the silicon substrate, then they are exposed to 0.1% silk in high pH condition and in low pH condition by submerging the substrate in the solution for 15minutes. Afterwards, the substrate is rinsed with nanopure water to remove the excess silk, and is dried with nitrogen gas. 0.1% silk pH was controlled with the addition of 0.1M NaOH and 0.1M HCl, and the pH of silk solution was confirmed using a pH probe.

## A.6 Mechanical buckling compression test

The nanocomposite film is released by dissolving the sacrificial PS layer with toluene, transferring released film to the PDMS block, and to clean silicon. The film on clean silicon was used to measure the film's thickness and the film on PDMS block was used to measure elastic modulus of the film. The PDMS with freestanding film is compressed with a buckling tool and its wavelength is collected to calculate the compressive tensile modulus of the chitin silk composite film.

# Appendix B

# Synthesis Methods

## B.1 Materials

Silk Cocoons were purchased from Mulberry Farms. Sodium Carbonate, Lithium Bromide, Hydrochloric acid (HCl), Sodium Hydroxide (NaOH), polystyrene, methanol, chitin, graphite flakes and 1,1,1,3,3,3-hexafluoro-2-propanol (HFIP) were purchased from Sigma Aldrich (St. Louis, MO, USA). TEM grids were purchased from Ted Pella (Redding, CA, USA). The water used in this work is Nanopure water (18.2 MΩ, Barnstead). Graphene oxide for adsorption study was purchased from cheap tubes.

## B.2 Silk Fibroin Preparation

Silk Fibroin was prepared from *Bombyx mori* silkworm cocoons using a reported protocol. [34] The layers from the cocoons were peeled away to assist in their dissolution in the process of degumming. After the dissolution and dialysis of the silk, the resulting solution was purified by twice centrifugation at 9000 rpm for 20 minutes at 4°C. The concentration of the resulting solution was 3.8 wt%. The solutions with desired concentrations were stored at 4°C and used within a month. The pH of the silk solutions was modified by adjusting the amount of HCl or NaOH.

## B.3 Graphene Oxide Preparation for composite

Graphene oxide is synthesized using improved method reported by Tour and co-workers. [35] 18g of $KMnO_4$ and 3 g of graphite flakes are placed in a 1L beaker. 9:1 mixture of concentrated $H_2SO_4/H_3PO_4$ (360:40mL) is added to the beaker. It produces exothermal heat of approximately 40°C. The beaker is placed on the hot plate (50°C) and the mixture is stirred for 12h at 100rpm. Then the reaction is cooled in the room temperature. After the reaction is cooled off, the mixture is mixed into ice (400mL) with 3mL of 30% $H_2O_2$. Reaction is cooled at room temperature and sift

through 300μm metal sieve to remove unexfoliated flakes. All the sifted mixture is placed into centrifuge tubes and centrifuged to remove the supernatant (7500rpm, 90mins). Resulting precipitates are washed using water (1X) and 30% HCl (1X) and centrifuged one more time (3000rpm, 90mins) then supernatants are removed to filter out multi-layered flakes. The precipitate is washed using water (1X), ethanol (1X) and water until the pH sets around 3.3. The resulting solution is centrifuged for the last time (5000rpm, 90min) and the precipitates are disperse in water.

## B.4 Chitin Solution Preparation

Chitin was dissolved using 1,1,1,3,3,3-hexafluoro-2-propanol (HFIP) in a glass vial since HFIP is such a strong organic solvent. To assist the dissolution process, the vial was placed in a sonication environment for two days. The concentration of the final solution was 0.3%. The chitin solution with desired concentrations were diluted into glass vials and stored at room temperature.

# Appendix C

# Supporting Information

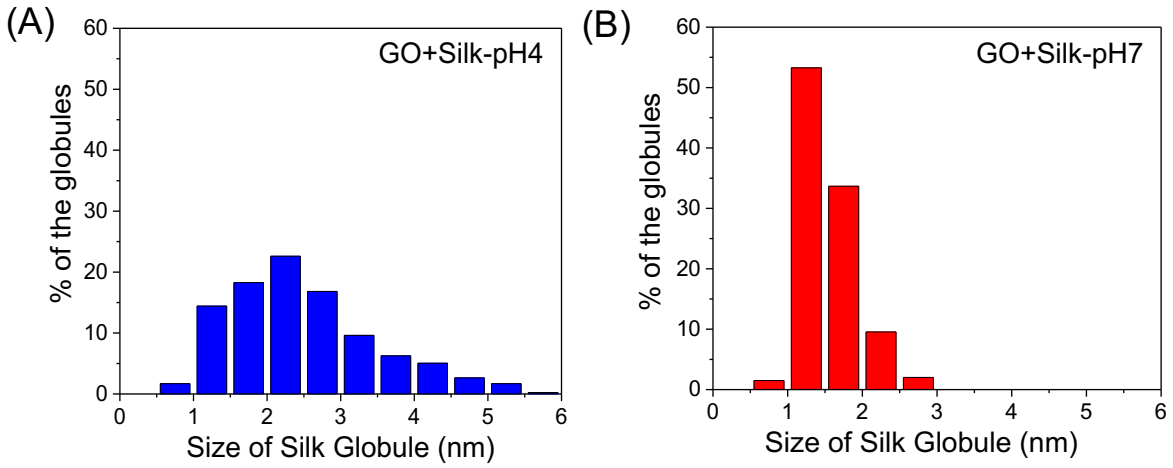


**Figure S.1- The size of the globules of silk adsorbed on GO varies as a function of the pH of silk solution. Globule size distribution computed from the AFM images of silk on GO showing the frequency counts of the globule size of silk at (A) pH 4 and (B) pH 7.**

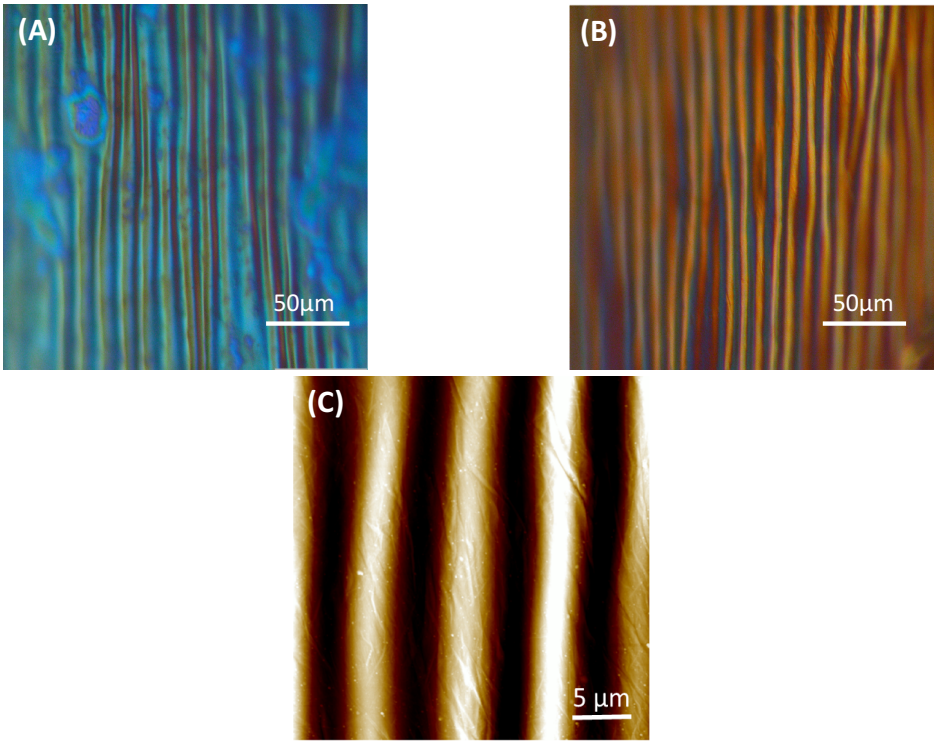


**Figure S.2 - Optical images of buckling pattern of GO-silk film (A) pH4 GO-Silk film (B) pH7 GO-Silk film (C) AFM image of the pH10 buckling pattern of the GO-silk film**

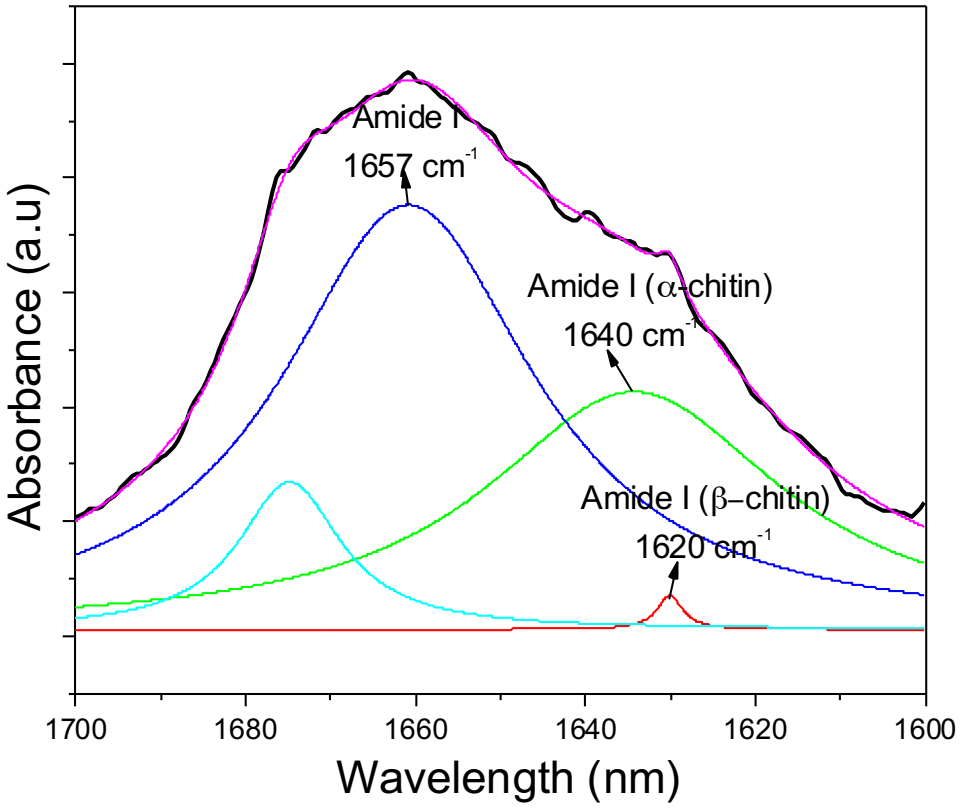


**Figure S.3- The amide peak deconvolution using Lorentzian peaks to estimate the relative amount of different conformations of chitin**

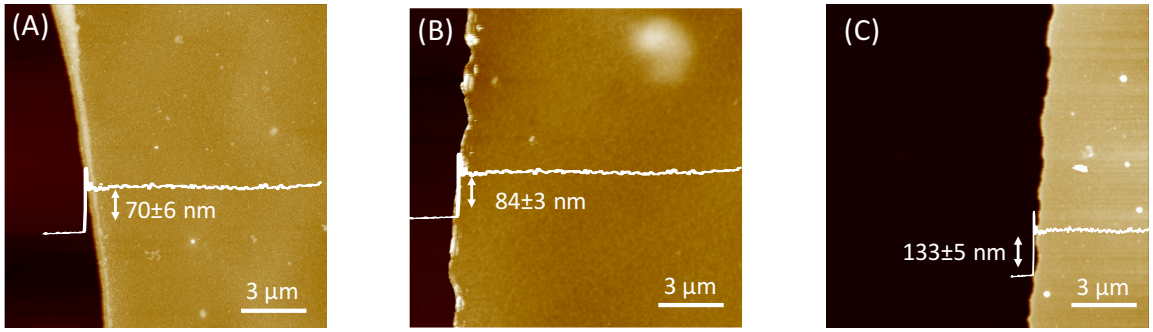


**Figure S.4- AFM images of thickness curves of the freestanding chitin silk film (A) 0.075% chitin silk (B) 0.15% chitin silk (C) 0.3% chitin silk**

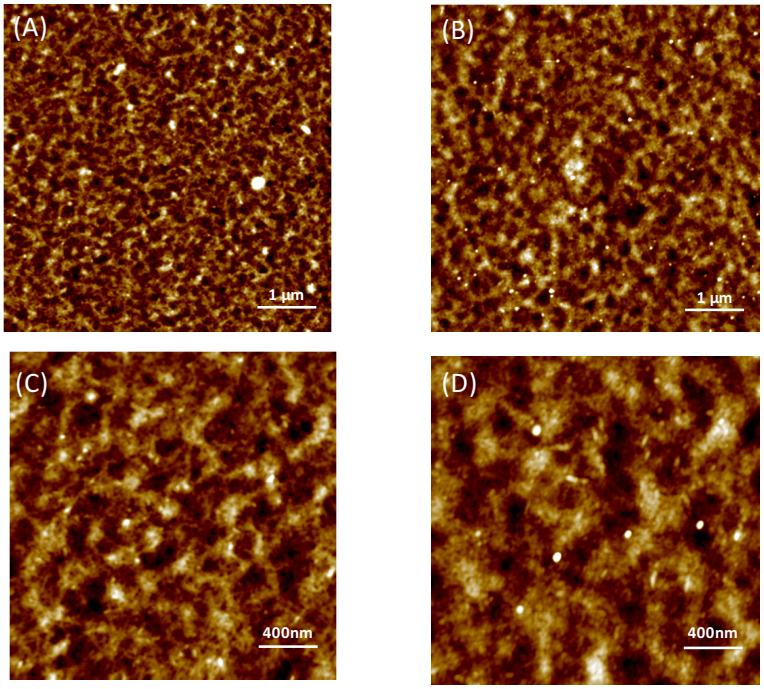


**Figure S.5- AFM images of thickness curves of the freestanding chitin silk film (A, C) 0.075% chitin silk (B, D) 0.3% chitin silk**

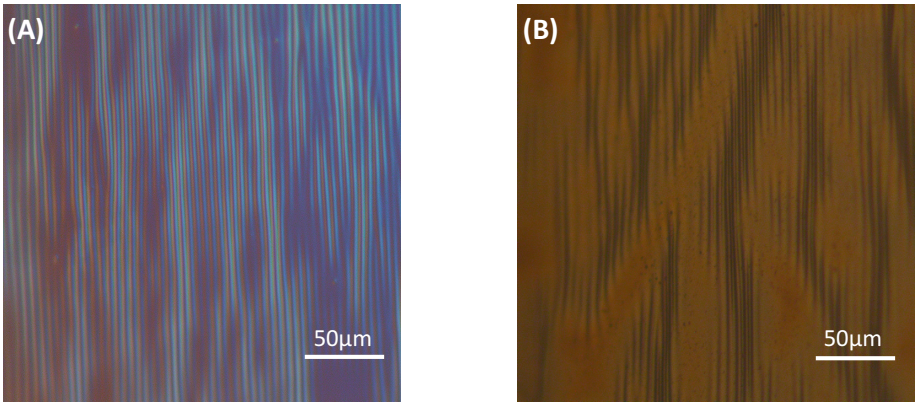


**Figure S.6 - Optical images of buckling patterns of chitin-silk film (A) 0.075% chitin-silk film (B) 0.15% chitin-silk film.**

# References


[1] Altman, G. H.; Diaz, F.; Jakuba, C.; Calabro, T.; Horan, R. L.; Chen, J.; Lu, H.; Richmond, J.; Kaplan, D. L., Silk-based biomaterials. *Biomaterials* **2003,** *24* (3), 401-416.

[2] (a) Chen, X.; Cai, H. F.; Ling, S. J.; Shao, Z. Z.; Huang, Y. F., Conformation Transition of Bombyx mori Silk Protein Monitored by Time-Dependent Fourier Transform Infrared (FT-IR) Spectroscopy: Effect of Organic Solvent. *Appl Spectrosc* **2012,** *66* (6), 696-699; (b) Hu, X.; Shmelev, K.; Sun, L.; Gil, E.-S.; Park, S.-H.; Cebe, P.; Kaplan, D. L., Regulation of Silk Material Structure by Temperature-Controlled Water Vapor Annealing. *Biomacromolecules* **2011,** *12* (5), 1686-1696.

[3] Matsumoto, A.; Chen, J.; Collette, A. L.; Kim, U.-J.; Altman, G. H.; Cebe, P.; Kaplan, D. L., Mechanisms of Silk Fibroin Sol−Gel Transitions. *The Journal of Physical Chemistry B* **2006,** *110* (43), 21630-21638.

[4] Vepari, Charu.; Kaplan, D.L. Silk as a Biomaterial. *Prog Polym Sci.* 2007 ; 32(8-9): 991–1007

[5] Hu, K.; Gupta, M. K.; Kulkarni, D. D.; Tsukruk, V. V. Ultra-Robust Graphene Oxide-Silk Fibroin Nanocomposite Membranes. *Advanced Materials* **2013**, *25*, 2301-2307.

[6] Yin, Y.; Hu, K.; Grant, A. M.; Zhang, Y.; Tsukruk, V. V. Biopolymeric Nanocomposites with Enhanced Interphases. *Langmuir* **2015**, *31*, 10859-10870.

[7] Naleway, S. E.; Porter, M. M.; McKittrick, J.; Meyers, M. A. Structural Design Elements in Biological Materials: Application to Bioinspiration. *Advanced Materials* **2015**, n/a-n/a.

[8] Tang, Z.; Kotov, N. A.; Magonov, S.; Ozturk, B. Nanostructured artificial nacre. *Nat Mater* **2003**, *2*, 413-418.

[9] Podsiadlo, P.; Kaushik, A. K.; Arruda, E. M.; Waas, A. M.; Shim, B. S.; Xu, J.; Nandivada, H.; Pumplin, B. G.; Lahann, J.; Ramamoorthy, A.; Kotov, N. A. Ultrastrong and Stiff Layered Polymer Nanocomposites. *Science* **2007**, *318*, 80-83.

[10] Das, P.; Malho, J.-M.; Rahimi, K.; Schacher, F. H.; Wang, B.; Demco, D. E.; Walther, A. Nacre-mimetics with synthetic nanoclays up to ultrahigh aspect ratios. *Nat Commun* **2015**, *6*.

[11] Li, X.; Xu, Z.-H.; Wang, R. In Situ Observation of Nanograin Rotation and Deformation in Nacre. *Nano Letters* **2006**, *6*, 2301-2304.

[12] Cai, W.; Piner, R. D.; Stadermann, F. J.; Park, S.; Shaibat, M. A.; Ishii, Y.; Yang, D.; Velamakanni, A.; An, S. J.; Stoller, M.; An, J.; Chen, D.; Ruoff, R. S. Synthesis and Solid-State NMR Structural Characterization of 13C-Labeled Graphite Oxide. *Science* **2008**, *321*, 1815-1817.

[13] Wan, S.; Peng, J.; Li, Y.; Hu, H.; Jiang, L.; Cheng, Q. Use of Synergistic Interactions to Fabricate Strong, Tough, and Conductive Artificial Nacre Based on Graphene Oxide and Chitosan. *ACS Nano* **2015**.

[14] Cui, W.; Li, M.; Liu, J.; Wang, B.; Zhang, C.; Jiang, L.; Cheng, Q. A Strong Integrated Strength and Toughness Artificial Nacre Based on Dopamine Cross-Linked Graphene Oxide. *ACS Nano* **2014**, *8*, 9511-951

[15] Altman, G. H.; Diaz, F.; Jakuba, C.; Calabro, T.; Horan, R. L.; Chen, J.; Lu, H.; Richmond, J.; Kaplan, D. L. Silk-based biomaterials. *Biomaterials* **2003**, *24*, 401-416.

[16] Hu, K.; Tolentino, L. S.; Kulkarni, D. D.; Ye, C.; Kumar, S.; Tsukruk, V. V. Written-in Conductive Patterns on Robust Graphene Oxide Biopaper by Electrochemical Microstamping. *Angewandte Chemie International Edition* **2013**, *52*, 13784-13788.

[17] Stafford, C. M.; Harrison, C.; Beers, K. L.; Karim, A.; Amis, E. J.; VanLandingham, M. R.; Kim, H.-C.; Volksen, W.; Miller, R. D.; Simonyi, E. E. A buckling-based metrology for measuring the elastic moduli of polymeric thin films. *Nat Mater* 2004, 3, 545-550.

[18] Genzer, J.; Groenewold, J. Soft matter with hard skin: From skin wrinkles to templating and material characterization. *Soft Matter* 2006, 2, 310-323.

[19] Singamaneni, S.; Tsukruk, V. V. Buckling instabilities in periodic composite polymeric materials. *Soft Matter* 2010, 6, 5681-5692

[20] Wegst, U. G. K.; Bai, H.; Saiz, E.; Tomsia, A. P.; Ritchie, R. O. Bioinspired structural materials. *Nat Mater* 2015, 14, 23-36.

[21] Ortiz, C.; Boyce, M. C. Bioinspired Structural Materials. *Science* 2008, 319, 1053-1054.

[22] Addadi, L.; Weiner, S. Biomineralization: A pavement of pearl. *Nature* 1997, 389, 912-915.

[23] Rolandi, M.; Rolandi, R. Self-assembled chitin nanofibers and applications. *Advances in Colloid and Interface Science* 2014, 207, 216-222.

[24] Cooper, A.; Zhong, C.; Kinoshita, Y.; Morrison, R. S.; Rolandi, M.; Zhang, M. Self-assembled chitin nanofiber templates for artificial neural networks. *Journal of Materials Chemistry* 2012, 22, 3105-3109.

[25] Zhong, C.; Deng, Y.; Roudsari, A. F.; Kapetanovic, A.; Anantram, M. P.; Rolandi, M. A polysaccharide bioprotonic field-effect transistor. *Nat Commun* 2011, 2, 476.

[26] Jayakumar, R.; Prabaharan, M.; Nair, S. V.; Tamura, H. Novel chitin and chitosan nanofibers in biomedical applications. *Biotechnology Advances* 2010, 28, 142-150.

[27] Smith, B. L.; Schaffer, T. E.; Viani, M.; Thompson, J. B.; Frederick, N. A.; Kindt, J.; Belcher, A.; Stucky, G. D.; Morse, D. E.; Hansma, P. K. Molecular mechanistic origin of the toughness of natural adhesives, fibres and composites. *Nature* 1999, 399, 761-763.

[28] Rinaudo, M. Chitin and chitosan: Properties and applications. *Progress in Polymer Science* 2006, 31, 603-632.

[29] Jang, M.-K.; Kong, B.-G.; Jeong, Y.-I.; Lee, C. H.; Nah, J.-W. Physicochemical characterization of α-chitin, β-chitin, and γ-chitin separated from natural resources. *Journal of Polymer Science Part A: Polymer Chemistry* 2004, 42, 3423-3432.

[30] Zhong, C.; Cooper, A.; Kapetanovic, A.; Fang, Z.; Zhang, M.; Rolandi, M. A facile bottom-up route to self-assembled biogenic chitin nanofibers. *Soft Matter* 2010, 6, 5298-5301.

[31] Vincent, J. F. V. Arthropod cuticle: a natural composite shell system. *Composites Part A: Applied Science and Manufacturing* 2002, 33, 1311-1315.

[32] Tadepalli, S.; Hamper, H.; Park, S. H.; Cao, S.; Naik, R. R.; Singamaneni, S. Adsorption Behavior of Silk Fibroin on Amphiphilic Graphene Oxide. *ACS Biomaterials Science & Engineering* 2016, 2, 1084-1092.

[33] Tsukada, M.; Gotoh, Y.; Nagura, M.; Minoura, N.; Kasai, N.; Freddi, G. Structural changes of silk fibroin membranes induced by immersion in methanol aqueous solutions. *Journal of Polymer Science Part B: Polymer Physics* 1994, 32, 961-968.

[34] Rockwood, D. N.; Preda, R. C.; Yucel, T.; Wang, X.; Lovett, M. L.; Kaplan, D. L. Materials fabrication from Bombyx mori silk fibroin. *Nat. Protocols* 2011, 6, 1612-1631.

[35] D. C. Marcano, D. V. Kosynkin, J. M. Berlin, A. Sinitskii, Z. Sun, A. Slesarev, L. B. Alemany, W. Lu, J. M. Tour. Improves synthesis of graphene oxide. *ACS Nano 2010*, 4, 4806.

# Vita

Sang Hyun Park

**Degrees**

M.S. Materials Science and Engineering — August 2016

B.S. Mechanical Engineering & Materials Science — May 2015

**Publications**

Biomimetic layer-by-layer composite of chitin and silk. 2016

Adsorption Behavior of Silk Fibroin on Amphiphilic Graphene Oxide. ACS Biomaterials Science and Engineering. 2016

Bioplasmonic Calligraphy for Multiplexed Label-free Biodetection. Biosensors and Bioelectronics. 2014